Metallic 1T-WS_2 for Selective Impedimetric Vapor Sensing

*Carmen C. Mayorga-Martinez, Adriano Ambrosi, Alex Yong Sheng Eng, Zdeněk Sofer, and Martin Pumera**

Selective gas sensing is of immense importance for industrial as well as safety purposes. Here it is shown that metallic 1T phase transition metal dichalcogenides, such as tungsten sulfide (WS_2), provide sensitive and selective platform for gas sensing. Using impedance spectroscopy distinguishable alterations can be detected on the impedance *phase* spectrum of interdigitated gold electrode modified with chemically exfoliated 1T-WS_2 caused by different vapors. In particular, it is found that the impedance *phase* spectra of 1T-WS_2 device present different resonant frequencies with maximum around 1 Hz in the presence of methanol vapor and around 1 kHz in the presence of water vapor. Such a well-distinguished signal allows their selective detection also when they are present in a mixture. The impedance *phase* spectra allow the selective methanol and water vapor sensing with an impedimetric device based on 1T-WS_2. This system utilizing 1T phase of WS_2 for selective gas sensing based on impedance spectroscopy opens new avenues for gas sensing and shall find wide spectra of applications.

1. Introduction

Various 2D materials have recently attracted much research interest as possible platforms for sensitive and selective gas or vapor sensing devices.[1] Among 2D materials, graphene has been one of the most explored for such purposes[2] but recently layered transition metal dichalcogenides (TMDs) showed promising possibilities for their employment in such applications.[3] Molybdenum[4] and tungsten[5] sulfides (MoS_2 and WS_2) are the most studied TMDs for gas sensing in a transistor[6] and resistor[7] configuration, due to their semiconductor behavior.[8]

The high sensitivity of gas sensing devices using different 2D materials has been demonstrated in several works but the ability to selectively detect different gases or vapors present in a mixture sample still remains a great challenge which was not sufficiently addressed previously. Selective detection was demonstrated only using pristine graphene transistor measuring low-frequency noise spectra[9] and with graphene/silicon heterojunction Schottky diode using electrochemical impedance spectroscopy measurements.[10] In the first method a complex data processing was required while in the second one the relative impedance change was referred to the *module* spectrum measured in vacuum. Here, we developed a selective vapor sensor using metallic 1T-WS_2 nanosheets (obtained by exfoliation of natural WS_2 with *tert*-butyllithium (*t*-Bu-Li) as intercalator) deposited onto interdigitated gold electrodes (see **Figure 1**) and recording impedance *phase* spectra. The resonance frequency (fr) is then used as distinctive parameter for a selective quantification of methanol and water vapors in isolated samples and mixtures.

One of the most common procedures to exfoliate layered TMD materials consists of a chemical intercalation of organolithium compounds in anhydrous solvents followed by a violent reaction with water which splits the sheets apart.[11] Different organolithium compounds (methyllithium, *n*-butyllithium, and *tert*-butyllithium) have been used and explored to produce single or few layer structures of different TMDs. It has been recently demonstrated that *n*-butyllithium and *tert*-butyllithium represent, with similar capabilities, the most effective intercalation agents.[12] Layered TMD materials generally exist with two possible polymorph structures: (i) 2H, most common for the naturally occurring materials, where the metal atom coordination is trigonal prismatic and (ii) 1T, where the metal atom coordination is octahedral. Beside structural differences the materials present significantly different electronic properties depending on their polymorph structures. The 2H phase confers semiconducting properties to the material while the 1T phase presents a metallic character with a significantly enhanced conductivity.[13] It has been demonstrated that Li intercalation followed by exfoliation induces a transition between the natural semiconducting 2H phase to the metallic 1T phase[14] although with different efficiencies depending on the TMD material employed.[15] 2H → 1T phase transition is particularly favored with WS_2 using *t*-Bu-Li intercalation compound.[15] With the intention to employ impedance spectroscopy as transducer technique we recognized the fundamental importance of the material conductivity, where one may expect improved sensitivity using a more conductive material. As such we opted to employ WS_2 nanosheets having an enhanced

Dr. C. C. Mayorga-Martinez, Dr. A. Ambrosi, A. Y. S. Eng, Prof. M. Pumera
Division of Chemistry and Biological Chemistry
School of Physical Mathematical Science
Nanyang Technological University
Singapore 637371, Singapore
E-mail: pumera.research@gmail.com
Prof. Z. Sofer
Department of Inorganic Chemistry
University of Chemistry and Technology Prague
Technicka 5, 166 28 Prague 6, Czech Republic

DOI: 10.1002/adfm.201502223

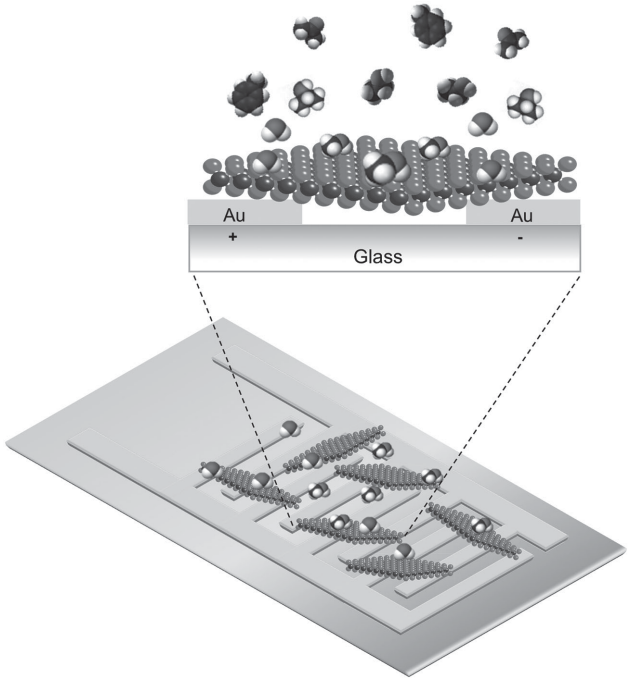

Figure 1. Schematic representation of interdigitated gold electrode modified with 1T-WS_2 nanosheets.

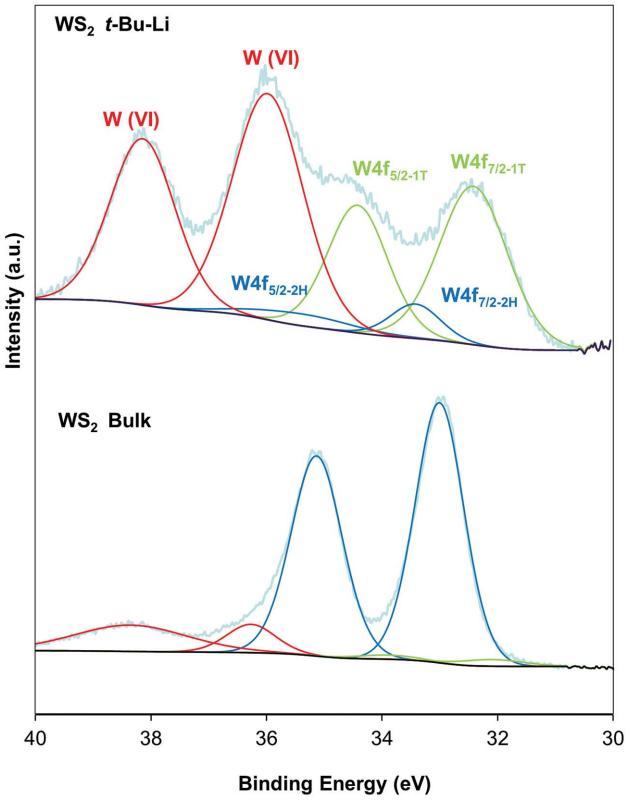

Figure 2. High-resolution XPS W 4f spectra of exfoliated 1T-WS_2 (top) and bulk natural WS_2 (bottom).

metallic character after the transition from 2H to 1T upon *t*-Bu-Li intercalation/exfoliation.

2. Results and Discussion

Raman spectroscopy confirmed the reduced number of layers upon exfoliation as can be seen in Figure S1 (Supporting Information). The in-plane $E_{2g}{}^1$ and out-of-plane A_{1g} modes at about 350 and 419 cm^{-1}, respectively, softened with respect to the spectrum of WS_2 in the bulk state, which indicates a reduced number of layers as well as a reduced lateral size of the sheets.[16] To further evaluate the exfoliation process, the specific surface area of the material was measured using the methylene blue adsorption method.[17] A surface area of 406.5 $m^2\ g^{-1}$ resulted after the exfoliation which is about 40 times larger than the surface area of WS_2 in its bulk state (10.2 $m^2\ g^{-1}$)[17] confirming an effective exfoliation procedure.

X-ray photoelectron spectroscopy (XPS) is particularly useful to identify the two polymorphs (2H and 1T) of TMD materials.[14] It has been observed that the components of the 1T phase in the high-resolution W4f spectrum appear at binding energies about 1 eV lower than those belonging to the 2H phase.[18] **Figure 2** shows high-resolution XPS spectrum of W4f for WS_2 in the bulk state and after exfoliation. It is clear that the material experienced a significant phase transition upon exfoliation presenting the components of the metallic 1T phase (at ≈32 and 34 eV) more prominent than those of the 2H phase (at ≈33 and 35 eV). WS_2 in the bulk state presents almost exclusively the components corresponding to the 2H phase. It should be noted that the signals recorded at 36 and 38 eV suggest the formation of W oxides (from the exfoliation).

In order to confirm the enhanced metallic character of WS_2 after exfoliation we performed impedance *module* measurements of the material before and after exfoliation using interdigitated gold electrode, which resulted with a decrease of the impedance *module* 50 times compared to the starting bulk material (see Figure S2 in the Supporting Information).

The 1T-WS_2 nanosheets obtained therefore offer high surface area for physisorption of different molecules as well as an enhanced metallic character which can be exploited for impedance spectroscopic measurements as explained below.

Electrochemical impedance spectroscopy is a powerful technique used especially for surface characterization[19] and bio/sensing detections.[20] More recently this technique was used for gas sensing with graphene/silicon heterojunction Schottky diode,[10] graphene oxide resistor,[21] and nanostructured zinc ferrite[22] thus demonstrating the versatility of this technique with different platforms. Here we study the selective effect of methanol and water vapors on the impedance spectra of 1T-WS_2 nanosheets deposited onto a standard interdigitated gold electrode and recorded in an environmental chamber (see scheme in Figure 1). Impedance *module* and *phase* plots were recorded in a frequency range of 1 mHz to 100 kHz using a sinusoidal AC potential perturbation of 0.01 V root mean square (rms) (see **Figures 3** and **4**).

Figure 3 shows that in the presence of methanol vapors the impedance *module* increases (blue curve) with respect to the bare electrode (light blue curve) in all the frequency range measured and is particularly evident at low frequencies. In

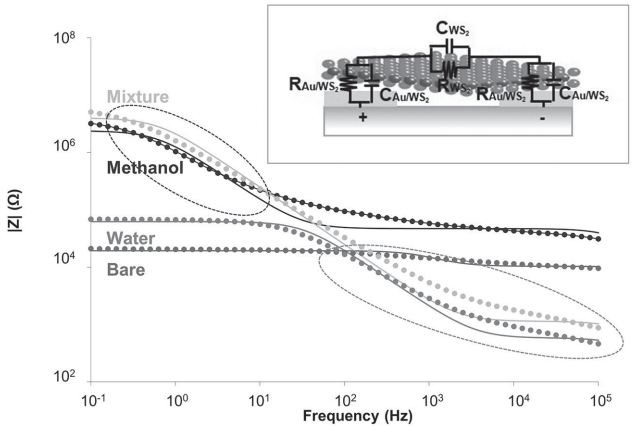

Figure 3. Experimental (scattered points) and simulated (solid line) data of impedance *module* of 1T-WS_2 in the absence (bare) and in the presence of 506 ppm methanol vapor, 26.6 g kg^{-1} water vapor and a mixture of both vapors. Inset: electrical equivalent circuit proposed for the modeled impedance *module* data.

the presence of water molecules, the impedance *module* also increases at low frequencies with respect to the bare electrode but not significantly while at high frequencies where there is a dramatic decrease of the impedance *module* (green curve). Consequently, when both molecules are present in a mixture sample, a significant increase of the impedance *module* is observed at low frequencies (due to methanol response) while at high frequencies a decreased impedance module is recorded (due to water response).

In order to understand the electrical behavior and the charge transport processes contributing to the variation of the impedance response, the experimental impedance data (scattered points) are modeled (solid lines) by using the simplified equivalent circuit shown in the inset of Figure 3, which allowed the best fit to our measurements. Considering the structure of this device, the model includes in series three parallel resistor-capacitor (*RC*) circuits, the first and the last one corresponding to the interface between gold electrode and WS_2 nanosheets ($C_{Au/WS2}$ and $R_{Au/WS2}$) while the second one corresponds to the interface between WS_2 nanosheets (C_{WS2} and R_{WS2}). Assuming

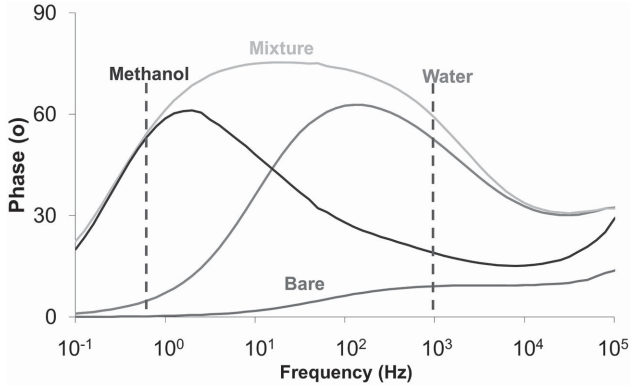

Figure 4. Impedance *phase* spectra of 1T-WS_2 platform bare and toward 506 ppm methanol vapor, 26.6 g kg^{-1} water vapor, and in the mixture of both vapors.

Table 1. Values of passive elements obtained from the electrical equivalent circuit proposed for modeled impedance data of 1T-WS_2 platform.

	Bare	Water	Methanol	Mixture
$R_{Au/WS2}$ (kΩ)	10.36	0.58	47.1	1.33
$C_{Au/WS2}$ (nF)	21.83×10^{-3}	1.22	21.16×10^{-3}	0.68
R_{WS2} (kΩ)	8.96	62.00	2522	3990
C_{WS2} (nF)	20.22	78.20	113.2	63.9

that the first and third *RC* circuit corresponds to the interface Au/WS_2, the total impedance could be expressed with the following equation:

$$|Z| = \frac{R_{Au/WS_2}}{1 + j\omega R_{Au/WS_2} C_{Au/WS_2}} + \frac{R_{WS_2}}{1 + j\omega R_{WS_2} C_{WS_2}} \quad (1)$$

The resulting fitting data are shown in **Table 1**.

In the presence of water vapor the resistance of the interface Au/WS_2 decreases while the capacitance increases compared with the blank measurements. Moreover, in the 1T-WS_2 nanosheets interface the resistance and the capacitance increases. On the other hand, in the presence of methanol the resistance of the interface Au/WS_2 increased 4.5 times with the capacitance unaltered, while in the interface of WS_2 nanosheets the resistance increased three orders of magnitude and the capacitance increased about 5.5 times. When the mixture of both vapors is measured, the resistance of Au/WS_2 interface decreases and the capacitance increases, similar to the impedance response observed in the presence of only water vapor. Considering the interface of WS_2 nanosheets, both the resistance and the capacitance increase, as occurred in the presence of methanol vapor. Using this data analysis we could ascertain that each vapor contributes in a different manner to the impedance response, allowing us to selectively and simultaneously detect both vapors (methanol and water) in one single measurement using the same device.

Similarly, the impedance *phase* spectra versus frequency present significantly different features when recorded in the presence of methanol or water. It can be seen in Figure 4 that in the presence of methanol a peak at resonant frequencies between 500 mHz and 1 Hz with maximum at about 1 Hz (blue curve) resulted. In the presence of water vapor the peak was recorded at frequencies between 50 Hz and 1 kHz (red curve) with maximum at about 500 Hz. Mixing both vapors resulted with a single broad peak between 500 mHz and 1 kHz (green curve) which indicates the simultaneous contribution of both vapors to the impedimetric response. Having the maximum responses distinctively separated, a direct vapor quantification was performed selecting a fixed frequency and monitoring the impedance *phase* changes. It is important to mention that when a similar sensing platform was prepared employing the bulk (2H phase) WS_2 material, no change was observed in the impedance response (*module* and *phase*) either in the absence and presence of the vapors (see Figure S3 in the Supporting Information), confirming the importance of the metallic character of the material and therefore the unique suitability of the metallic 1T phase of WS_2.

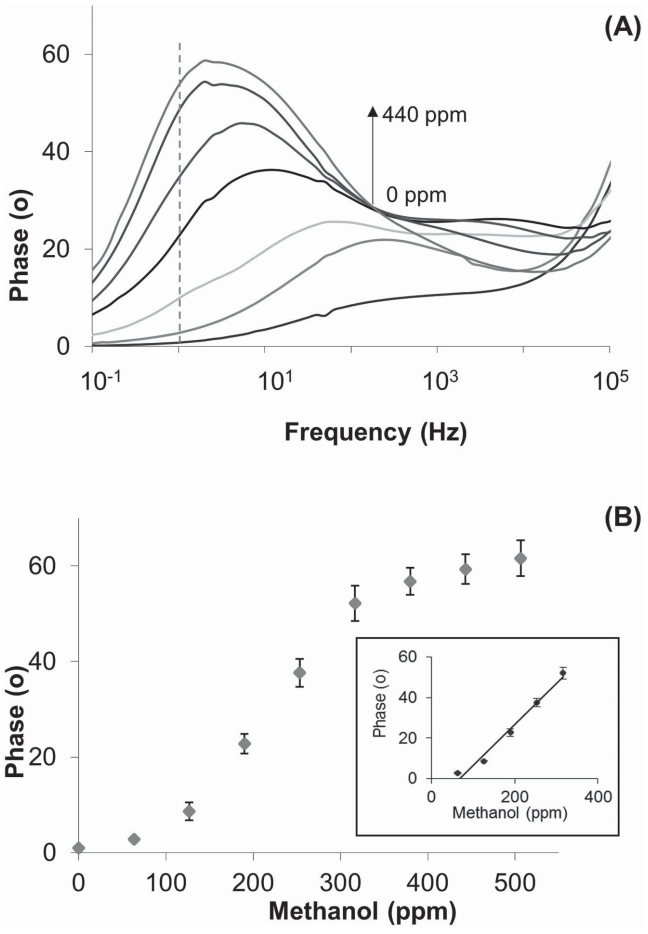

Figure 5. A) Impedance *phase* spectra of 1T-WS_2 platform upon different methanol vapor concentration. B) Impedance *phase* at 1 Hz as a function of different methanol vapor concentration. Inset: calibration curve of methanol vapors.

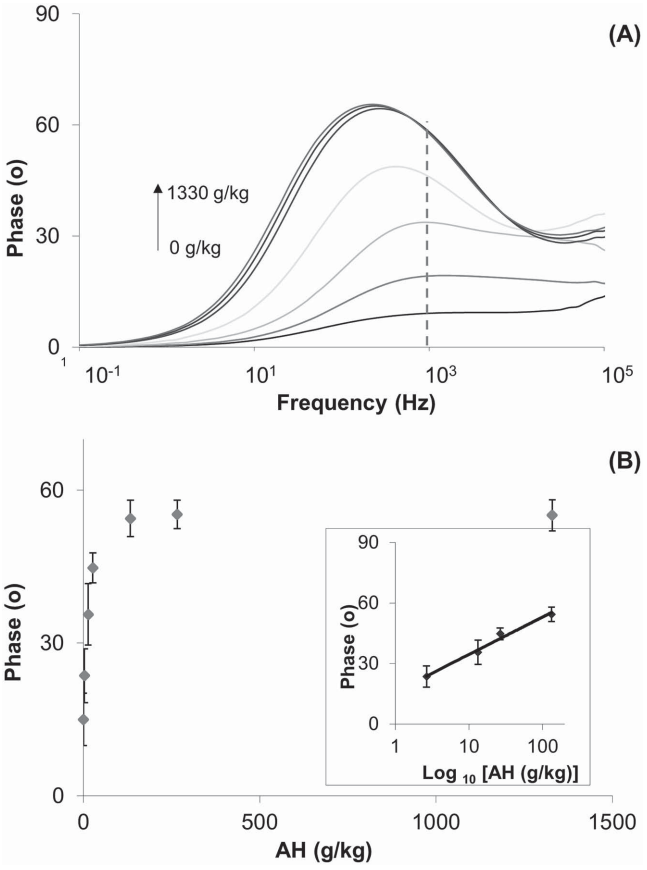

Figure 6. A) Impedance *phase* spectra of 1T-WS_2 toward different AH. Different AH as a function of impedance *phase* measurements at 1 kHz. Inset: calibration curve of AH.

In order to quantify the methanol vapor, 1T-WS_2 based sensor is exposed to the vapor generated by different methanol concentrations. **Figure 5**A shows the *phase* impedance spectra obtained with different methanol concentrations and Figure 5B summarizes the impedance phase values recorded at the fixed frequency of 1 Hz as a function of methanol concentration. It can be seen in Figure 5 that when the methanol concentration is increased the impedance *phase* also increases until it reaches saturation for concentrations higher than 380 ppm. The linear response is thus defined between 63 and 317 ppm methanol (see inset of Figure 5B) with r = 0.9904. These measurements are reproducible with relative standard deviation (RSD) of 8% measured using three different sensors. Further, this system is very sensitive with a low limit of detection (LOD) of 5.6 ppm, which is around 45 times below of the occupational exposure limits of methanol established by the National Institute for Occupational Safety and Health (NIOSH) of USA.[23]

Consequently, water vapor is quantified in the same way, with the spectrum of impedance *phase* increasing when the absolute humidity (AH) increases (**Figure 6**A). The absolute humidity (g kg^{-1}) measured at room temperature (25 °C) is defined by the mass of the water vapor (m_w) in a certain volume (V_{air}), which can be expressed as

$$AH = m_w/V_{air} \quad (2)$$

The response of impedance *phase* measured at 1 kHz as a function of absolute humidity is shown in Figure 6B. The system reaches saturation at absolute humidity values higher than 133 g kg^{-1} showing a linear response between 3 and 133 g kg^{-1} of AH with r = 0.9923 (see inset in Figure 6B). High reproducibility and sensitivity of this system for water sensing are observed with RSD of 14% and low LOD of 1.9 g kg^{-1}. Using the humidity content tables,[23] the LOD reported in this study is 10% in terms of relative humidity.

The reusability of this sensor for water and methanol sensing are also evaluated. After the sensors are exposed to the corresponding vapor, they are cleaned at 100 °C for 10 min. As it can be seen in Figure S4A (Supporting Information), the sensors exposed to water recover to the original signal after the thermal treatment. The calibration of water vapor is performed using the same 1T-WS_2 platform with successive measurements falling within 7% RSD (see Figure S4B in the Supporting Information). Once exposed to methanol; however, the sensor failed to recover to the original impedance phase value after the thermal treatment indicating a stronger interaction

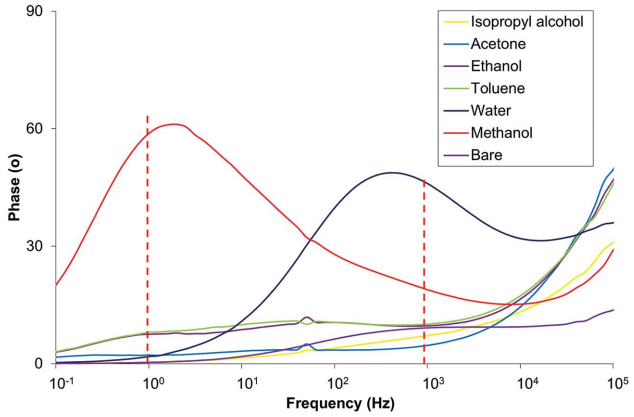

Figure 7. Selectivity studies of 1T-WS_2 platform toward 1394 ppm toluene, 1268 ppm acetone, 1264 ppm ethanol, 1259 ppm isopropyl alcohol, 380 ppm methanol, and 27 g kg^{-1} water.

between WS_2 and methanol (see Figure S5 in the Supporting Information).

With demonstration of the sensor's ability to detect water and methanol, we then proceeded to investigate its selectivity in the presence of a complex sample mixture. We recorded the impedance *phase* spectra of 1T-WS_2 sensor in the presence of a sample containing 1394 ppm toluene, 1268 ppm acetone, 1264 ppm ethanol, 1259 ppm isopropyl alcohol, 380 ppm methanol, and 27 g kg^{-1} water (see **Figure 7**). The concentrations of the interference species have been chosen to be in excess compared with the amount of water and methanol vapors. It can be seen that even in such situations the sensor responds selectively only to water and methanol and with negligible responses toward interfering species.

3. Conclusion

In summary, it was found that the impedance *phase* spectra of 1T-WS_2 present specific resonant frequencies for methanol and water vapors, meaning that using the same 1T-WS_2 platform we are able to detect methanol and water vapors by selecting specific frequencies (1 Hz for methanol and 1 kHz for water). The impedance response of 1T-WS_2 is modeled by a proposed equivalent circuit that describes the resistive and capacitive behaviors. The impedance *phase* of 1T-WS_2 measured at a certain frequency for each vapor enables highly selective gas sensing and this system can be used as a reliable, sensitive, and reproducible tool for methanol and water vapor detection. Moreover, this system could be converted into a portable and automated system for vapor sensing since it makes use of a simple electrochemical detection scheme which does not require complex data processing. Such simple but selective 1T-WS_2 based sensor is expected to lead the way for real world gas sensing application.

4. Experimental Section

Exfoliation of WS_2 (obtained from Alfa Aesar, Germany) was performed following the protocol previously described.[12] Suspensions of 3 g of WS_2 bulk powder in 20 mL of 1.7 M *tert*-butyllithium (Sigma-Aldrich, Czech Republic) in pentane was carried out. The solution was then stirred for 72 h at 25 °C under argon atmosphere. The Li-intercalated material was separated by suction filtration under argon atmosphere and the intercalation compound was washed several times with hexane (dried over Na). The separated TMDs with intercalated Li was placed in water (100 mL) and repeatedly centrifuged (18 000 g). The obtained material was dried in vacuum oven at 50 °C for 48 h prior to further use.

In a glass chamber of 312 mL volume with a tight closing, the solution of study was placed at desired volumes. The electrical connector for interdigitated electrode was previously adapted in the chamber cover in a way to avoid any contact with the solution. The interdigitated gold electrode (width 10 µm, spacing 5 µm; purchased from ALS Co., Japan) was modified with 1 µL of WS_2 *t*-Bu-Li exfoliated dispersed in deionized water at concentration of 1 mg mL^{-1}. The electrode was then dried under a lamp for 20 min, leaving a randomly deposited material film on the interdigitated area bridging the two Au electrode bands.

The impedance measurements were carried out at room temperature using an Autolab302 potentiostat/galvanostat/frequency-response analyzer PGST30 controlled by General Purpose Electrochemical System/Frequency Response Analysis (GPES/FRA) software Version 4.9, and a sinusoidal potential modulation of ±10 mV amplitude in the 0.1 Hz to 100 kHz frequency range with logarithmic scale of 10 points per decade was applied. XPS was performed with a Phoibos 100 spectrometer and a monochromatic Mg X-ray radiation source (SPECS, Germany). High-resolution spectra for W 4f were collected using the C 1s signal at 284.5 eV for calibration. Raman spectra were obtained by using a confocal micro-Raman LabRam HR instrument from Horiba Scientific in backscattering geometry with a charge coupled device (CCD) detector, a 514.5 nm Ar laser, and a 100x objective mounted on a Olympus optical microscope. The calibration is initially made using a silicon reference at 520 cm^{-1} and gives a peak position resolution of less than 1 cm^{-1}.

Supporting Information

Supporting Information is available from the Wiley Online Library or from the author.

Acknowledgement

M.P. acknowledges Tier 2 grant (MOE2013-T2-1-056) from Ministry of Education, Singapore. Z. S. was supported by Czech Science Foundation (GACR project no. 15-07912S.

Received: June 1, 2015
Revised: July 16, 2015
Published online: August 10, 2015

[1] S. Some, Y. Xu, Y. Kim, Y. Yoon, H. Qin, A. Kulkarni, T. Kim, H. Lee, *Sci. Rep.* **2013**, *3*, 1868.
[2] a) S. Some, Y. Xu, Y. Kim, Y. Yoon, H. Qin, A. Kulkarni, T. Kim, H. Lee, *Sci. Rep.* **2013**, *3*, 1868; b) R. A. Potyrailo, C. Surman, N. Nagraj, A. Burns, *Chem. Rev.* **2011**, *111*, 7315; c) F. Schedin, A. K. Geim, S. V. Morozov, E. W. Hill, P. Blake, M. I. Katsnelson, K. S. Novoselov, *Nat. Mater.* **2007**, 652.
[3] D. Sarkar, X. Xie, J. Kang, H. Zhang, W. Liu, J. Navarrete, M. Moskovits, K. Banerjee, *Nano Lett.* **2015**, *15*, 2852.
[4] a) D. Sarkar, X. Xie, J. Kang, H. Zhang, W. Liu, J. Navarrete, M. Moskovits, K. Banerjee, *Nano Lett.* **2015**, *15*, 2852; b) S. Zhao, J. Xue, W. Kang, *Chem. Phys. Lett.* **2014**, *595–596*, 35; c) A. L. Friedman, F. K. Perkins, E. Cobas, G. G. Jernigan, P. M. Campbell, A. T. Hanbicki, B. T. Jonker, *Solid-State Electron.*

2014, *101*, 2; d) M. Donarelli, S. Prezioso, F. Perrozzi, F. Bisti, M. Nardone, L. Giancaterini, C. Cantalinib, L. Ottaviano, *Sens. Actuator, B* **2015**, *207*, 602; e) D. J. Late, Y. K. Huang, B. Liu, J. Acharya, S. N. Shirodkar, J. Luo, A. Yan, D. Charles, U. V. Waghmare, V. P. Dravid, C. N. R. Rao, *ACS Nano* **2013**, *7*, 4879; f) Q. Yue, Z. Shao, S. Chang, J. Li, *Nanoscale Res. Lett.* **2013**, *8*, 1; g) D. J. Late, T. Doneux, M. Bougouma, *Appl. Phys. Lett.* **2014**, *105*, 233103.

[5] a) M. O'Brien, K. Lee, R. Morrish, N. C. Berner, N. McEvoy, C. A. Woldend, G. S. Duesberg, *Chem. Phys. Lett.* **2014**, *615*, 6; b) N. Huo, S. Yang, Z. Wei, S.-S. Li, J.-B. Xia, L. Li, *Sci. Rep.* **2014**, *4*, 1.

[6] a) D. Sarkar, X. Xie, J. Kang, H. Zhang, W. Liu, J. Navarrete, M. Moskovits, K. Banerjee, *Nano Lett.* **2015**, *15*, 2852; b) Q. He, Z. Zeng, Z. Yin, H. Li, S. Wu, X. Huang, H. Zhang, *Small* **2012**, *8*, 2994; c) A. L. Friedman, F. K. Perkins, E. Cobas, G. G. Jernigan, P. M. Campbell, A. T. Hanbicki, B. T. Jonker, *Solid-State Electron.* **2014**, *101*, 2; d) D. J. Late, Y. K. Huang, B. Liu, J. Acharya, S. N. Shirodkar, J. Luo, A. Yan, D. Charles, U. V. Waghmare, V. P. Dravid, C. N. R. Rao, *ACS Nano* **2013**, *7*, 4879; e) M. O'Brien, K. Lee, R. Morrish, N. C. Berner, N. McEvoy, C. A. Woldend, G. S. Duesberg, *Chem. Phys. Lett.* **2014**, *615*, 6; f) N. Huo, S. Yang, Z. Wei, S.-S. Li, J.-B. Xia, L. Li, *Sci. Rep.* **2014**, *4*, 1.

[7] M. Donarelli, S. Prezioso, F. Perrozzi, F. Bisti, M. Nardone, L. Giancaterini, C. Cantalini, L. Ottaviano, *Sens. Actuator, B* **2015**, *207*, 602.

[8] Q. H. Wang, K. Kalantar-Zadeh, A. Kis, J. N. Coleman, M. S. Strano, *Nat. Nanotechnol.* **2012**, *7*, 669.

[9] S. Rumyantsev, G. Liu, M. S. Shur, R. A. Potyrailo, A. A. Balandin, *Nano Lett.* **2012**, *12*, 2294.

[10] A. Fattah, S. Khatami, C. C. Mayorga-Martinez, M. Medina-Sánchez, L. Baptista-Pires, A. Merkoçi, *Small* **2014**, *10*, 4193.

[11] a) M. Chhowalla, H. S. Shin, G. Eda, L.-J. Li, K. P. Loh, H. Zhang, *Nat. Chem.* **2013**, *5*, 263; b) A. Ambrosi, Z. Sofer, M. Pumera, *Small* **2015**, *11*, 605.

[12] a) A. Ambrosi, Z. Sofer, M. Pumera, *Small* **2015**, *11*, 605; b) A. Y. S. Eng, A. Ambrosi, Z. Sofer, P. Šimek, M. Pumera, *ACS Nano* **2014**, *8*, 12185; c) C. C. Mayorga-Martinez, A. Ambrosi, A. Y. S. Eng, Z. Sofer, M. Pumera, *Elecrochem. Commun.* **2015**, *56*, 24.

[13] M. Chhowalla, H. S. Shin, G. Eda, L.-J. Li, K. P. Loh, H. Zhang, *Nat. Chem.* **2013**, *5*, 263.

[14] G. Eda, H. Yamaguchi, D. Voiry, T. Fujita, M. Chen, M. Chhowalla, *Nano Lett.* **2011**, *11*, 5111.

[15] A. Ambrosi, Z. Sofer, M. Pumera, *Chem. Commun.* **2015**, *51*, 8450.

[16] H. S. S. Ramakrishna Matte, A. Gomathi, A. K. Manna, D. J. Late, R. Datta, S. K. Pati, C. N. R. Rao, *Angew. Chem. Int. Ed.* **2010**, *49*, 4059.

[17] A. Y. S. Eng, A. Ambrosi, Z. Sofer, P. Šimek, M. Pumera, *ACS Nano* **2014**, *8*, 12185.

[18] B. Mahler, V. Hoepfner, K. Liao, G. A. Ozin, *J. Am. Chem. Soc.* **2014**, *136*, 14121.

[19] B. Y. Chang, S.-M. Park, *Annu. Rev. Anal. Chem.* **2010**, *3*, 207.

[20] a) B.-Y. Chang, S.-M. Park, *Annu. Rev. Anal. Chem.* **2010**, *3*, 207; b) C. C. Mayorga-Martinez, L. Hlavata, S. Miserere, A. López-Marzo, J. Labuda, J. Pons, A. Merkoçi, *Biosens. Bioelectron.* **2014**, *55*, 355; c) C. C. Mayorga-Martinez, A. Chamorro-Garcia, A. Merkoçi, *Biosens. Bioelectron.* **2015**, *67*, 53; d) G. C. Jiménez, S. Eissa, A. Ng, H. Alhadrami, M. Zourob, M. Siaj, *Anal. Chem.* **2015**, *87*, 1075; e) J. S. Daniels, N. Pourmand. *Electroanalysis* **2007**, *19*, 1239; f) A. Bonanni, M. Pumera, *ACS Nano* **2011**, *5*, 2356; g) L. Rivas, C. C. Mayorga-Martinez, D. Quezada-Gonzales, A. Zamora, A. de la Escosura-Muñiz, A. Merkoçi, *Anal. Chem.* **2015**, *87*, 5167; h) A. H. Loo, A. Bonanni, A. Ambrosi, H. L. Poh, M. Pumera, *Nanoscale* **2012**, *4*, 921.

[21] S. Borini, R. White, D. Wei, M. Astley, S. Haque, E. Spigone, N. Harris, J. Kivioja, T. Ryhänen, *ACS Nano* **2013**, *7*, 11166.

[22] P. K. Kannan, R. Saraswathi, *Talanta* **2014**, *129*, 545.

[23] The National Institute for Occupational Safety and Health (NIOSH), Methanol: Systemic Agent, http://www.cdc.gov/niosh/ershdb/emergencyresponsecard_29750029.html, accessed: May, 2015.

[24] DEVATEC, Humidity Content tables, http://www.devatec.com/humidity/pdf/Learn_more_on_Humidification.pdf, accessed: May, 2015.